Available online at www.sciencedirect.com

ScienceDirect

Proceedings of the Combustion Institute 000 (2022) 1–10

Proceedings of the Combustion Institute

www.elsevier.com/locate/proci

Simultaneous side-wall-schlieren and -emission imaging of autoignition phenomena in conventional and constrained-reaction-volume shock-tube experiments

Adam J. Susa*, Ronald K. Hanson

Stanford University, Department of Mechanical Engineering, Stanford, CA, USA

Received 6 January 2022; accepted 23 August 2022
Available online xxx

Abstract

Simultaneous schlieren and emission imaging through the side wall of a round shock tube is reported for application to experimental autoignition studies. A round, optically accessible shock tube featuring windows designed as aberration-corrected cylindrical lenses provides a large side-wall field of view compatible with both emission and schlieren imaging. Autoignition experiments are reported for non-dilute propane–oxygen–argon mixtures ($\phi = 1$ C_3H_8 in 21% O_2, 79% Ar) at temperatures (T_5) spanning the range 1,203–1,438 K and pressures near 1 atm. Experiments are performed using both conventional and constrained-reaction-volume (CRV) filling, allowing for the most detailed comparison to date of ignition dynamics between these two types of experiments. When T_5 exceeds 1,290 K, strong ignition is observed to initiate in the immediate proximity of the end wall regardless of the filling strategy. In lower-T_5 experiments, mild ignition is observed to initiate spontaneously at remote locations, which often exceeding the imaging FOV in conventional experiments but are constrained within about 5 cm of the end wall in CRV experiments. Measured ignition delay times (IDTs) are compared to predictions from three kinetic mechanisms. IDTs simulated using the San Diego and USC Mech II mechanisms are of the same magnitude as the measurements but exhibit a lower activation energy; the propane submechanism from NUIG 1.1, meanwhile, systematically over predicts observed IDTs by roughly a factor of two. Comparisons are also made between the experimental measurements and predictions from a recently introduced 1-D axial-temperature-gradient model describing remote ignition in shock tubes. Considering the effect of a supposed $dT_5/dz = 150$ K/m gradient, the 1-D model functionally predicts the remote ignition observed in $T_5 < 1{,}290$ K experiments and suggests the use of CRV filling may significantly reduce the error introduced into IDT measurements by remote ignition at low-T_5 conditions.

Keywords: Shock tube; Schlieren; Chemiluminescence; Autoignition; Ignition delay time

1. Introduction

For nearly as long as shock tubes have been used in the study of autoignition, imaging has been em-

* Corresponding author.
E-mail address: asusa@alumni.stanford.edu (A.J. Susa).

https://doi.org/10.1016/j.proci.2022.08.063
1540-7489

ployed to provide insights into the dynamics of experiments. In one of the first shock-tube imaging studies, Strehlow and Cohen performed schlieren streak imaging through slit windows in a round shock tube to study ignition of hydrogen (H_2) in oxygen (O_2) [1]. Voevodsky and Soloukhin used streak imaging to identify a regime of mild ignition that gave rise to large discrepancies in ignition delay times (IDT, τ_{ign}) [2]. Meyer and Oppenheim used high-speed schlieren imaging in a rectangular shock tube to inform their identification of the criteria $\left(\partial \tau_{\text{ign}}/\partial T\right)_P < -2$ μs/K as predictive of the boundary separating the strong and mild ignition regimes [3].

Through the years that followed, the use of schlieren imaging continued, primarily using square shock tubes. In a study of engine-relevant fuels, Fieweger et al. observed both an initial, inhomogeneous stage of ignition consisting of deflagrative kernels and a subsequent deflagration-to-detonation transition (DDT) [4]. Brown and Thomas visually compared the effects of dilution with argon (Ar) and nitrogen (N_2) [5]. The facility used in that work utilized a valve in the driven section and an inert buffer gas to prevent "spurious" ignition, a variation on a technique employed by [1] and now known as the constrained-reaction-volume (CRV) method [6,7].

Troutman et al. kicked off a wave of chemiluminescence imaging studies with a method of imaging through an optical shock-tube end wall [8]. The utility of emission imaging for diagnosing inhomogeneous ignition and compatibility of the technique with existing facilities are factors underlying the method's rapid adoption and subsequent widespread use [*e.g.*, [9–15]]. Recently, applications of dual-perspective emission imaging performed though the end and side walls of round shock tubes have been reported using numerous experimental configurations. Ninnemann et al. added an annular quartz optical section to their facility [16], Figueroa-Labastida and Farooq implemented high-aspect-ratio slot windows [17], Nativel et al. used a custom endoscope [18], and Susa et al. imaged through a conventional side-wall port [19].

In the present work, simultaneous schlieren and chemiluminescence imaging of autoignition phenomena is reported for the first time. The unique side-wall imaging flame test section (SWIFT) provides optical access to the round shock tube. Experiments performed using conventional and CRV filling are reported, providing a comparison of autoignition behavior between the two methodologies. Details of the present experimental setup are provided in Section 2, followed by a presentation of the imaging results (Section 3). Aggregated results of experiments are discussed in Section 4 in relation to their comparison with 0-D ignition simulations and a 1-D model of ignition in the presence of an axial temperature gradient predictive of the observed remote-ignition behavior.

2. Experimental methods

2.1. Facility and instrumentation

Autoignition experiments are performed in a high-purity, constrained-reaction-volume (CRV) kinetics shock tube, a facility recently modified with the introduction of the SWIFT to enable large-FOV, side-wall schlieren imaging. The driver section and driven section up to the CRV gate valve remain as reported by Campbell et al. [7]. The 9.7-m driven section features a 11.5-cm-inner diameter; the 3.6-m driver section is of larger diameter, but annular inserts are used to reduce the effective diameter to match that of the driven section. A driver insert, designed in simulation using StanShock [20], was used to counteract effects of dP/dt to provide near-constant post-reflected-shock pressures prior to ignition [21].

The SWIFT, as instrumented for the present investigation, is shown in cross section in Fig. 1. The 6061-T6 aluminum section features hard-anodized, matte black surfaces to minimize reflections. The side-wall windows, designed as afocal, cemented-doublet, cylindrical lenses with an inner radius matching the contour of the tube, provide a 5- by 18-cm field of view. Geometries of the inner fused-silica and outer BK-7 elements were selected to correct cylindrical aberrations, making the windows compatible with schlieren imaging. An inset end-wall assembly (Fig. 1a) positions the end wall about 1 mm within the view of the side-wall windows. Additional details of the SWIFT facility can be found in [22, Ch. 6]

Schlieren imaging is performed laterally through the side wall windows using a modified Z-fold arrangement comprised of 4-inch-diameter off-axis-parabolic (OAP) mirrors (30°, $f = 32.7$ cm) [23]. A green, high-power light-emitting diode (LED) paired with a 0.5-mm pinhole provides the light source; a 1-mm pinhole positioned at the second focal point served as the schlieren stop, producing an isotopic response to density gradients [24]. Schlieren images are recorded by a Phantom v2012 camera at 100,000 frames per second (fps) using a 512- by 336-pixel sensor region with a short (1–3 μs) exposure time. Distortion introduced by the optical configuration and characterized using a dot-grid target is corrected through "warp" functionality provided by Scikit-Image [23,25]. Schlieren image resolution is 56 pix/cm over a 8.5- by 5-cm field of view (FOV).

Emission imaging is performed at an angle through a side-wall window to avoid interfering with the schlieren optics. A Phantom v710 camera captures images through a 430-nm band-pass filter to isolate emission from CH^* radicals. The long-working-distance arrangement enables a 18.5- by 4.6-cm FOV to be imaged by a 256- by 128-pixel sensor region (13 pix/cm) at 200,000 fps. Primary exposure times of 1–4.6 μs were long enough to

Please cite this article as: A.J. Susa and R.K. Hanson, Simultaneous side-wall-schlieren and -emission imaging of autoignition phenomena in conventional and constrained-reaction-volume shock-tube experiments, Proceedings of the Combustion Institute, https://doi.org/10.1016/j.proci.2022.08.063

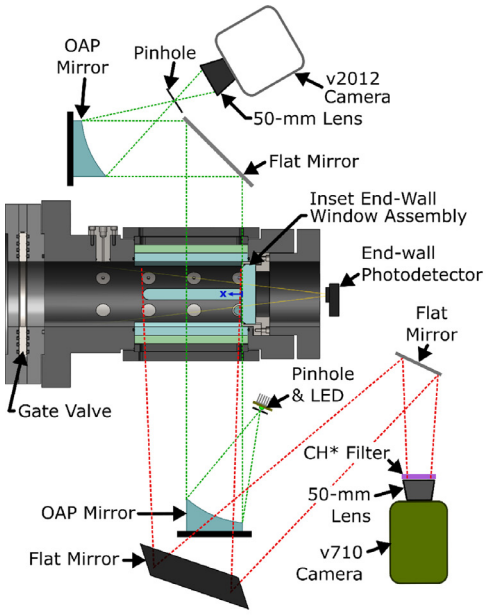

(a) Top-down view

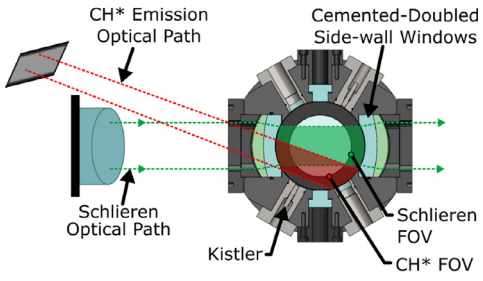

(b) Axial view

Fig. 1. Experimental configuration for simultaneous side-wall emission and schlieren imaging in the SWIFT. (a) Top-down view showing all components of the imaging systems. (b) Axial cross-sectional view showing only the last mirror of imaging systems, with shaded regions in the tube indicating the overlapping fields of view (approximate) for the emission (red) and schlieren (green) diagnostics. (For interpretation of the references to color in this figure legend, the reader is referred to the web version of this article.)

capture weak emission at the onset of spontaneous ignition. The extreme-dynamic-range (EDR) exposure was set to 0.2–1 μs to prevent image saturation from intense detonations. Distortion correction using a dot-grid target is applied to remove both optical distortion associated with the windows and rotation induced by the turning mirrors.

A suite of conventional diagnostics completes the experimental setup. Four fast-response PCB pressure transducers distributed along the SWIFT are recorded to determine the incident shock speed used as an input to a normal-shock equation solver (FROSH) to calculate the post-reflected-shock (region-5) conditions [26]. A Kistler pressure transducer 3 mm from the inset end wall provides high fidelity pressure–time (P–t) measurements. A 3.41-μm laser-absorption diagnostic [27] provides *in situ* verification of the fuel loading. An ultraviolet-(UV-)sensitive photodetector was used to record end-wall emission signals. While IDT determinations based on these conventional diagnostics are beyond the scope of the present work, plots of data recorded in each experiment are provided for reference in Supplement 1.

2.2. Image interpretation

Here, the image processing applied to the schlieren and emission videos is described. Videos saved in raw "cine" format are read using pycine [28] and processed using open-source tools from Scikit-Image [25]. All final figures and videos were generated using Matplotlib [29].

Following distortion correction, schlieren images are background corrected through their conversion to optical density (OD), which is calculated pixel-wise as $\mathrm{OD}_k = -\ln(I_k/I_{\mathrm{bkgd}})$. Here, values I_k and I_{bkgd} represent pixel intensities of video frame k and a pre-shock background image, respectively. OD image values are zero where $I = I_{\mathrm{bkgd}}$ and positive for the typical case of $I < I_{\mathrm{bkgd}}$ for schlieren images. In practice, a small amount of jitter in the intensities of schlieren images is observed when short exposure times are used, an artifact removed by subtracting the median OD_k value from each frame.

The treatment of CH* emission images recorded on a dark background is quite straightforward. Following distortion correction, background subtraction was employed utilized a global median over all dimensions of the image sequence. Emission intensities were then globally normalized, producing relative emission levels on the range 0 to 1.

For compact presentation in print, image sequences are converted to synthetic streak (z–t) images by collapsing the vertical image axis, producing a 2-dimensional image in which the horizontal axis represents axial distance (z) and the vertical axis corresponds to time (t). In the figures that follow, schlieren and emission z–t images are overlaid to create composite streak images, in which the absolute value of the mean OD is shown for schlieren values and the maximum intensity is taken for emission images to preserve the normalization and facilitate visualization of weakly emitting regions.

Ignition times (t_{ign}) and locations (z_{ign}) are determined from the z–t images. Ignition criteria are defined as the time and location at which the relative emission intensity first reaches a critical value (e). Three criteria ($e \in \{0.1, 0.2, 0.5\}$) are evaluated

Please cite this article as: A.J. Susa and R.K. Hanson, Simultaneous side-wall-schlieren and -emission imaging of autoignition phenomena in conventional and constrained-reaction-volume shock-tube experiments, Proceedings of the Combustion Institute, https://doi.org/10.1016/j.proci.2022.08.063

in Section 3, represented on z–t diagrams as green, yellow, and red stars, respectively. In Section 4, measured values corresponding to the earliest onset of ignition (*i.e.*, $e = 0.1$) are compared to model predictions.

2.3. Experimental conditions and test-gas filling

Experiments were performed using a test-gas mixture comprised of stoichiometric ($\phi = 1$) propane (C_3H_8) in an oxidizer of 21% O_2 and 79% Ar. Ignition was observed at region-5 temperatures (T_5) in the range 1,203–1,438 K near atmospheric pressure (0.98–1.05 atm). Both conventionally and CRV-filled experiments are reported, providing a direct comparison of ignition behaviors observed with each method.

In conventionally filled experiments, the entire 9.7-m-long driver section is filled with test-gas mixture. In CRV experiments, the driven section is filled with the CRV gate valve closed, allowing the 40-cm test section to be filled with test-gas and the buffer section to be filled with an acoustically tailored, density-matched mixture of propane, Ar, and N_2 [7,12][1]. After filling each section, the pressures of the buffer and test sections are equilibrated through the filling manifold. The gate valve is opened just prior to diaphragm rupture (*i.e.*, within seconds) to minimize the time available for diffusive or gravity-current-induced mixing of the buffer and test gases [12]. In the present CRV experiments, no evidence of test-gas dilution or stratification was observed.

The shock waves compress the test gas, of initial extent, L_1 (9.7 m for conventional fill, 40 cm for CRV), to a region-5 length, $L_5 = L_1(\rho_1/\rho_5)$. For typical density ratios $\rho_1/\rho_5 \approx 8$, $L_5 \approx 1.2$ m is typical for conventionally filled experiments, such that the test gas extends well beyond the imaging FOV. For CRV experiments, however, $L_5 \approx 5$ cm making the entire extent of the test gas observable in both the schlieren and emission FOVs.

3. Imaging results

In this section, experimental imaging results are presented as composite streak images and discussed. Across all images, schlieren OD values are represented by gray; emission intensities are overlaid in red. The driven-side end wall is located at the right edge; times are shown relative to the shock wave reflecting from the end wall. Fig. 2a is annotated to show the extents of the schlieren and emission FOVs. Triangles mark the arrival of the incident and reflected shocks at the PCB locations; solid lines trace the inferred shock positions. The nominal location of the test–buffer contact surface is shown as a brown dash-dot line in CRV z–t diagrams. In addition to the z–t images presented here, full videos for all experiments are provided in the supplementary materials.

3.1. Conventionally filled experiments

Fig. 2 displays composite z–t images for conventionally filled experiments, illustrating a transition in the ignition mode and location as T_5 is reduced. In the highest-T_5 experiments (1,423 K in Fig. 2a and 1,390 K in S2g), ignition initiates adjacent to the end wall in what can be readily classified as "strong" ignition [3]. This mode of ignition is ideal for shock-tube IDT measurements, as the region-5 conditions are precisely known at the end wall and "time zero" from which ignition is referenced is precisely defined as the time of shock reflection.

At somewhat lower T_5 (1,271–1,343 K), ignition occurs in a more distributed manner. In Fig. 2b and c (and S2h), weak levels of emission are first observed about 2 cm from the end wall. In Fig. 2d, emission is first detected farther from the wall, near 8 cm. Looking to the full-frame videos (S2b–d, h), localized regions of expansion can be seen in the schlieren recordings about 10 μs preceding the first observance of emission at those same locations. The local homogeneity and consistent structure of these expanding regions do not align with the expected stochastic appearance of deflagrations ignited by a hot particles [10] or pockets of gas [*e.g.*, 30, 31]. Instead, the observations support an interpretation of these remote ignition events as having been spontaneously induced by zero-dimensional (0-D) chemistry, a possibility revisited in the later discussion Section 4.2.

Following the onset of ignition (green stars), emission is observed over a distributed region before coalescing into a discrete detonation fronts. In Fig. 2b and c, detonations are seen as the thin red line angling upward to the left in z–t images. In Fig. 2d, detonations form traveling in both directions, with the right-traveling front producing a reflected shock upon reaching the end wall.

In the two lowest-T_5 experiments, the loci of the first detected emission are found even farther from the end wall (Fig. 2e and f). At 1,228 K (Fig. 2e), emission is first detected near 10 cm. Looking to the full video (S2e), disturbances are seen to enter the schlieren frame from beyond its FOV. That observation, combined with the apparent presence of a second ignition front initiating outside the emission FOV, complicates the determination of the mechanism responsible for inducing ignition. The interpretation of the 1,210-K (2 f) experiment is more evident; the ignition front entering the emission FOV from the side clearly indicates that the onset of ignition occurred at $z_{ign} > 18.5$ cm prior to its detection in the images.

[1] Non-ideal results from an experiment with an untailored buffer gas are presented and discussed in supplements S1.4 and S4 to illustrate the importance of buffer-gas tailoring.

Please cite this article as: A.J. Susa and R.K. Hanson, Simultaneous side-wall-schlieren and -emission imaging of autoignition phenomena in conventional and constrained-reaction-volume shock-tube experiments, Proceedings of the Combustion Institute, https://doi.org/10.1016/j.proci.2022.08.063

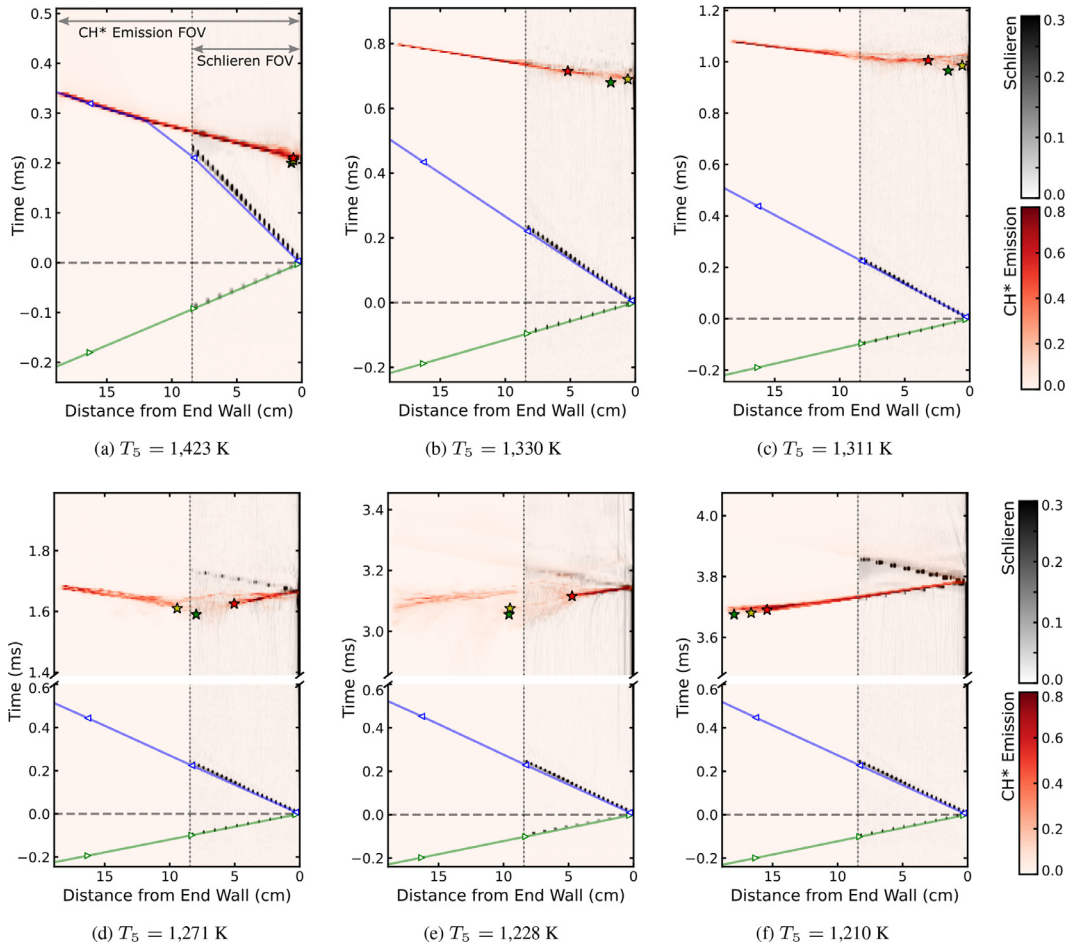

Fig. 2. Composite synthetic streak images of CH* emission (red) overlaid on schlieren records (gray) from six C_3H_8-O_2-Ar ($\phi = 1$) autoignition experiments using conventional shock tube filling. Times are shown relative to the shock reflecting from the end wall; broken time axes are used in (d-f) to show only the time ranges of interest. The extent of the schlieren images is indicated in (a). Incident (green) and reflected (blue) shock trajectories are overlaid, as determined from PCB data (triangle markers). Stars (⋆) mark the times and location of ignition, defined as the first instance of the relative emission reaching a critical value, e: green = 0.1, yellow = 0.2, red = 0.5. Full videos of convention-fill experiments are provided as supplements (S2a–h). (For interpretation of the references to color in this figure legend, the reader is referred to the web version of this article.)

3.2. CRV Experiments

Fig. 3 presents the composite z–t image results of autoignition experiments performed using CRV filling. Notable differences are evident in the CRV ignition experiments as compared to those using conventional filling. At the three highest T_5 conditions (1,342–1,438 K, Fig. 3a–c), strong ignition develops spontaneously in close proximity to the end wall. The ignition fronts propagate away from the end wall until they reach the buffer–gas contact surface (brown dash-dot line), where the reaction terminates but a shock wave is transmitted.

At a lower T_5 of 1,299 K (Fig. 3d), emission is first detected about 2 cm from the end wall following spontaneous expansion visible in the schlieren video (S3d). More intense emission is then first observed adjacent to the wall; the lack of transmitted shock beyond the contact surface indicates that the ignition front does not undergo DDT. Another experiment at this same T_5 condition (S3g) exhibits remarkable similarity to that shown in Fig. 3d, demonstrating the repeatability of the experiments and supporting a 0-D-chemistry interpretation of the ignition mechanism.

In the CRV experiments with the lowest T_5 (1,203–1,247 K, Fig. 3e and f), ignition occurs in a mild, spatially distributed manner over an extended duration. This behavior differs from that observed in conventionally filled experiments at comparable

Please cite this article as: A.J. Susa and R.K. Hanson, Simultaneous side-wall-schlieren and -emission imaging of autoignition phenomena in conventional and constrained-reaction-volume shock-tube experiments, Proceedings of the Combustion Institute, https://doi.org/10.1016/j.proci.2022.08.063

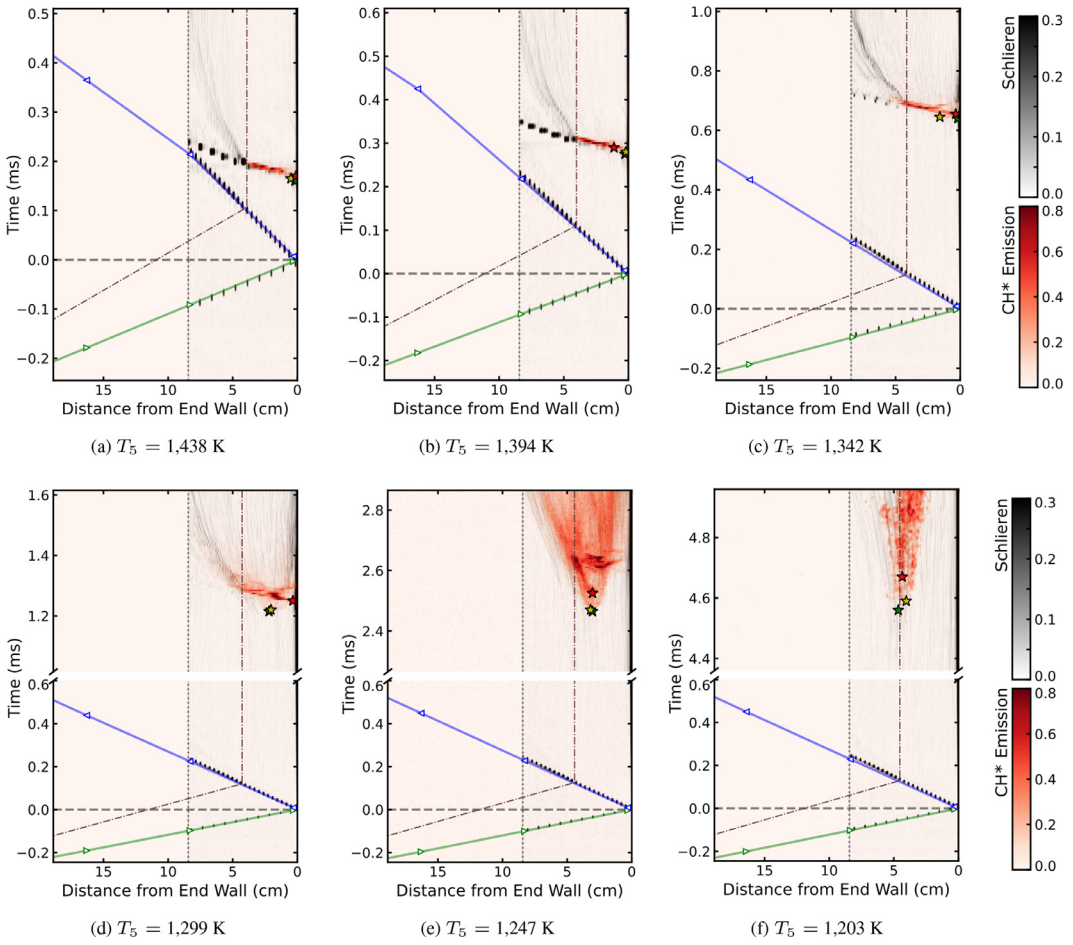

Fig. 3. Composite synthetic streak images of CH* emission (red) overlaid on schlieren records (gray) from six C_3H_8-O_2-Ar (ϕ= 1) autoignition experiments with CRV shock tube filling. Times are shown relative to the shock reflecting from the end wall; broken time axes are used in (d-f) to show only the time ranges of interest. The brown dash-dot line traces the nominal path of the test–buffer contact surface, which stagnates at L_5. Incident (green) and reflected (blue) shock trajectories are overlaid, as determined from PCB data (triangle markers). Stars (⋆) mark the times and location of ignition, defined as the first instance of the relative emission reaching a critical value, e: green = 0.1, yellow = 0.2, red = 0.5. Videos of CRV experiments are provided as supplements S3a–g. (For interpretation of the references to color in this figure legend, the reader is referred to the web version of this article.)

T_5 (Fig. 2d–f) in which mild ignition led to the development of detonations. The differing ignition behaviors are likely attributable to the nature of flow confinement in experiments using different filling methodologies. The limited axial extent of reactive mixture in CRV experiments allows the test gas to expand more freely than in conventionally filled experiments, such that the confining effect required for DDT to occur may not be present; the presence of CH* emission beyond the nominal contact surface location in Fig. 3e and f confirms the presence of an expanded test-gas region. In the complete videos (S3e and S3f), it is apparent that the distributed nature of the onset of emission is not consistent with a deflagration, suggesting instead that an interpretation of ignition being induced by spontaneous, 0-D chemistry cannot be ruled out. In these experiments, deflagrations do appear to spread outward from the initial ignition location, controlling the spread of emission at later times.

4. Discussion

Ignition times (t_{ign}) and locations (z_{ign}) determined from the 8 conventionally filled and 7 CRV experiments using the $e = 0.1$ threshold (green stars in z–t diagrams) are aggregated in Fig. 4. The choice of the lowest e threshold reflects a desire to capture the initial, apparently spontaneous onset

Please cite this article as: A.J. Susa and R.K. Hanson, Simultaneous side-wall-schlieren and -emission imaging of autoignition phenomena in conventional and constrained-reaction-volume shock-tube experiments, Proceedings of the Combustion Institute, https://doi.org/10.1016/j.proci.2022.08.063

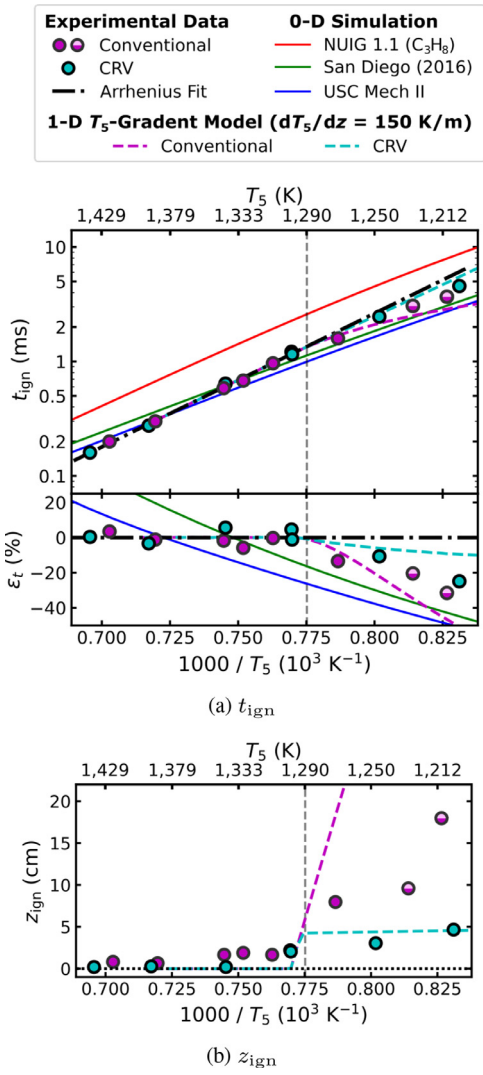

(a) t_{ign}

(b) z_{ign}

Fig. 4. Ignition results extracted from emission images using an $\epsilon = 0.1$ criteria. Markers represent experiments: solid-filled when the onset occurs within the imaging FOV and half-filled markers when evidence of ignition initiating outside the FOV is present. (a) Measured t_{ign} (top) and residuals (ϵ_t, bottom) calculated against an Arrhenius fit of $T_5 > 1{,}290$ K data (black dash-dot line). Also shown are τ_{ign} values from 0-D simulations (solid lines) performed with a constant-*HP* reactor model. (b) z_{ign} inferred from composite streak images. In both subplots, predictions of a 1-D axial-temperature-gradient model [22] calculated using a $\mathrm{d}T_5/\mathrm{d}z = 150$ K/m gradient are shown as dashed lines.

of ignition. More intense emission levels tend to result from subsequent phenomena, such as DDT, not immediately relevant to the characterization of autoignition chemistry. Half-filled markers are used to represent the two lowest-T_5 conventional-fill experiments, recalling evidence that ignition initiated outside the imaging FOV at an earlier t_{ign} and larger z_{ign} than plotted.

4.1. IDT comparison to 0-D simulations

The top axis of Fig. 4a presents an Arrhenius diagram of t_{ign} values measured relative to the shock-wave reflection from the end wall. Measurements are overlaid on τ_{ign} values simulated using a 0-D, constant-enthalpy–pressure (-*HP*) model in Cantera [32] with ignition defined by a ΔT of 500 K. Three kinetic mechanisms — the propane sub-mechanism from NUIG 1.1 [33], the propane mechanism from UC San Diego [34], and USC Mech II [35] — are evaluated through the comparison of their predicted τ_{ign} to the present measurements. Also shown is an Arrhenius fit to t_{ign} values from $T_5 > 1{,}290$ K experiments, the range over which the onset of ignition occurred near the end wall ($z_{\mathrm{ign}} \lesssim 2$ cm in Fig. 4b).

The bottom axis of Fig. 4a shows residuals (ϵ_t) of the measured t_{ign} and simulated τ_{ign} values calculated against the Arrhenius fit, τ_{Arr}:

$$\epsilon_t = \left(t_{\mathrm{ign}} - \tau_{\mathrm{Arr}}\right)/\tau_{\mathrm{Arr}}. \tag{1}$$

Over the range $T_5 > 1{,}290$ K, t_{ign} measured in conventional and CRV experiments are found to be consistent with one other and well described by the Arrhenius expression, exhibiting residuals of about 5% or less. The agreement of simulated τ_{ign} values, however, is less than stellar. Values τ_{ign} simulated using the San Diego and USC Mech II are generally of the correct magnitude but exhibit a weaker T_5 dependence (*i.e.*, lower activation energy) than seen in the data; this leads to the mechanisms over predicting t_{ign} by more than 20% at $T_5 > 1{,}400$ K and under predicting t_{ign} by a similar amount for $T_5 < 1{,}290$ K. Despite its extensive validation, the NUIG 1.1 propane sub-mechanism performs even worse, over predicting t_{ign} by roughly a factor of 2 across the $T_5 > 1{,}290$ K range but with a T_5 dependence that more closely aligns with the measurements.

4.2. 1-D temperature-gradient model

At temperatures below 1,290 K, measured values t_{ign} values are found to be shorter than expected based on the Arrhenius fit (Fig. 4a), coinciding with z_{ign} being found farther from the end wall (Fig. 4b). Mechanisms such as burning particles [10] and hot spots arising from the boundary layer [*e.g.*, 30, 31] have been discussed in the literature as being responsible for locally igniting deflagrations away from the end wall. However, the present imaging results reveal that ignition appears to initiate spontaneously and not from a singular ignition point. This finding suggests that even remote ignition events observed in this work may have been induced by 0-D chemistry, a notion requiring deeper consideration.

Please cite this article as: A.J. Susa and R.K. Hanson, Simultaneous side-wall-schlieren and -emission imaging of autoignition phenomena in conventional and constrained-reaction-volume shock-tube experiments, Proceedings of the Combustion Institute, https://doi.org/10.1016/j.proci.2022.08.063

A typical expectation of shock-tube experiments holds that the test gas nearest the end wall, being the first to pass through the reflected shock and reach region-5 conditions, has the longest time to react and should therefore be the first to ignite when ignition is induced by 0-D chemistry. Importantly, this expectation is premised on an assumption that the thermodynamic state of the region-5 test gas is uniform.

Here, the effect of relaxing the uniform-test-gas assumption is evaluated in relation to the present experiments through a presumed presence of an axial temperature gradient ($\mathrm{d}T_5/\mathrm{d}z$) in the test gas. The basis for axial temperature variation in shock tubes dates at least as far back as Belford and Strehlow, who noted that shock attenuation produces a gradient in the post-shock conditions [36]; later works suggested a temperature gradient may be related to remote ignition without investigating the premise further [*e.g.*, 6, 37]. Recently, Lipkowitz *et al.* identified the presence of $\mathrm{d}T_5/\mathrm{d}z$ of $\mathcal{O}(100$ K/m) in simulations of shock-tube autoignition experiments, which they identified as a cause of remote ignition in those simulations [38].

The predicted effect of imposing a T_5 gradient of $\mathrm{d}T_5/\mathrm{d}z = 150$ K/m was evaluated using the 1-D temperature-gradient model reported by Susa [22, pp. 257–267]. Results of the 1-D model are shown in Fig. 4 as dashed lines; colors correspond to the filling method. Briefly, the model assumes that ignition initiates at location z_{ign} within the test gas (*i.e.*, $z_{\mathrm{ign}} \leq L_5$) of minimum lab-frame ignition time, t_{ign}:

$$t_{\mathrm{ign}}(z) = t_{\mathrm{r}}(z) + \tau_{\mathrm{ign}}(T_5(z)) \tag{2}$$

$$= \frac{z}{V_{\mathrm{r}}} + \tau_{\mathrm{ign}}\left(T_5^0 + z\frac{\mathrm{d}T_5}{\mathrm{d}z}\right). \tag{3}$$

Here, $t_{\mathrm{r}}(z)$ is the lab-frame time for the reflected shock (velocity V_{r}) to reach z. $\tau_{\mathrm{ign}}(T_5(z))$ is the IDT evaluated at the local temperature $T_5(z)$. T_5^0 is the temperature at the end-wall, which is plotted as the horizontal axes in Fig. 4. In applying the model to the present experiments, the empirical Arrhenius fit (τ_{Arr}) is used to evaluate τ_{ign}.

Looking first to the z_{ign} plot (Fig. 4b), it is seen that the 1-D model predicts remote ignition to occur when $T_5 < 1,300$ K. In modeled results using conventional filling, the predicted z_{ign} increases rapidly, exceeding the values observed in the experiments. Notable, however, is that the predicted location exceed the emission FOV for $T_5^0 < 1{,}270$ K, consistent with the evidence of ignition beyond the FOV in the two lowest-T_5 conventional-fill experiments. In CRV experiments, the predicted z_{ign} is limited by the shorter extent L_5 of test gas, closely matching the transition observed in the experiments from ignition at the end wall to ignition near the contact surface.

The predicted effect of T_5-gradient-induced remote ignition on measured t_{ign} is shown in Fig. 4a. For $T_5^0 > 1{,}290$ K, t_{ign} predicted with $\mathrm{d}T_5/\mathrm{d}z$ coincides with τ_{Arr}, a result of ignition at or very near the end wall. At lower T_5^0, predicted values of t_{ign} are shorter than the 0-D τ_{Arr} due to ignition occurring remotely at a location of locally higher T_5. The magnitude of the error in t_{ign} compared to τ_{Arr} resulting from remote ignition is predicted by the $\mathrm{d}T_5/\mathrm{d}z$ model to be much smaller in CRV experiments ($\sim$10%) than those using conventional fill (reaching $>$ 50%). Experimentally determined t_{ign} show less distinction between filling methods than predicted, though the suspected onset of ignition beyond the FOV (and at earlier t_{ign} than observed) in the low-T_5, conventionally filled experiments impedes direct comparison to CRV results for which the time and location of ignition is clearly observable.

The deviation of the CRV results from τ_{Arr} by more than the magnitude predicted by the 1-D model could have any number of explanations. One likely factor is non-Arrhenius behavior in the IDT, which is evident in the simulated values but not considered in the Arrhenius fit used to apply the 1-D model. Only a small amount of fall off in the underlying, ground-truth τ_{ign} values would be required at low-T_5 conditions to bring the 1-D model in line with t_{ign} measured in CRV experiments. Another likely possibility is that the $\mathrm{d}T_5/\mathrm{d}z$ gradient is not accurately described by a constant value across all experimental conditions, with variation across different T_5 conditions likely; differences between filling methods is also a possibility. As such, while the 1-D model predictions are functionally predictive of the observed ignition behavior, additional investigation into the presence, magnitude, and nature of $\mathrm{d}T_5/\mathrm{d}z$, in particular experimental-condition and facility dependencies, would broadly benefit the understanding and interpretation of shock-tube autoignition experiments.

5. Conclusion

Simultaneous side-wall-schlieren and -emission imaging of shock-tube autoignition experiments was reported for the first time in experiments performed using conventional and CRV filling. This novel diagnostic technique revealed significant differences in the ignition dynamics between the two methods. Qualitative observations revealed that even at conditions exhibiting remote ignition, the onset of ignition occurred in a locally homogeneous manner suggestive of initiation by spontaneous autoignition chemistry.

Quantitative experimental measurements of t_{ign} and z_{ign} were extracted from synthetic z–t diagrams generated from video sequences. Extracted values t_{ign} for high-T_5 experiments not affected by remote ignition were found to be consistent between the

Please cite this article as: A.J. Susa and R.K. Hanson, Simultaneous side-wall-schlieren and -emission imaging of autoignition phenomena in conventional and constrained-reaction-volume shock-tube experiments, Proceedings of the Combustion Institute, https://doi.org/10.1016/j.proci.2022.08.063

conventional- and CRV-filled experiments and well described by an Arrhenius fit (within about 5%). Comparing the high-T_5 measurements to 0-D simulations, τ_{ign} values predicted by the San Diego [34] and USC Mech II [35] mechanisms were found to be of roughly the correct magnitude but exhibited a lower activation energy than suggested by the measurements; a propane submechanism from NUIG 1.1 [33] was found to systematically over predict the measured t_{ign} by roughly a factor of two.

Measurements of both t_{ign} and z_{ign} were also compared to predictions of a recently proposed 1-D axial-temperature-gradient model. Considering the effect of a supposed dT_5/dz of 150 K/m, remote ignition is correctly predicted for $T_5 <$ 1,290 K. The 1-D model additionally predicts measured t_{ign} values falling below $\tau_{ign}(T_5^0)$ when remote ignition is present. Model results indicate use of the CRV method should effectively mitigate the measurement-error magnitude at low-T_5 conditions. Further investigation to confirm the presence and nature of dT_5/dz in shock tube experiments promises to inform improved methods and interpretations of autoignition experiments and thus enable improved kinetic mechanisms that rely upon such measurements in their development.

Declaration of Competing Interest

The authors declare that they have no known competing financial interests or personal relationships that could have appeared to influence the work reported in this paper.

Acknowledgments

This work was supported by the U.S. National Science Foundation under award number 1940865, contract monitor Dr. John Daily. Instrumentation used in this work was funded by the U.S. Army Research Office under award number W911NF-20-1-006, contract monitor Dr. Ralph Anthenien.

Supplementary material

Raw data and additional experimental details are provided to supplement this work:

- S1 Additional experimental data (S1.1 and S1.2), ignition-induced pressure rise (S1.3), and results from an untailored CRV experiment (S1.4)
- S2 Videos of conventional-fill experiments (S2a–h)
- S3 Videos of CRV experiments (S3a–g)
- S4 Video of an untailored CRV experiment

Supplementary material associated with this article can be found, in the online version, at 10.1016/j.proci.2022.08.063

References

[1] R.A. Strehlow, A. Cohen, Initiation of detonation, Phys. Fluids 5 (1962) 97–101.
[2] V. Voevodsky, R. Soloukhin, On the mechanism and explosion limits of hydrogen-oxygen chain self-ignition in shock waves, in: Proc. Combust. Inst, volume 10, 1965, pp. 279–283.
[3] J. Meyer, A. Oppenheim, On the shock-induced ignition of explosive gases, in: Symp. (Intl.) Combust., volume 13, Elsevier, 1971, pp. 1153–1164.
[4] K. Fieweger, R. Blumenthal, G. Adomeit, Self-ignition of SI engine model fuels: a shock tube investigation at high pressure, Combust. Flame 109 (4) (1997) 599–619.
[5] C. Brown, G. Thomas, Experimental studies of shock-induced ignition and transition to detonation in ethylene and propane mixtures, Combust. Flame 117 (4) (1999) 861–870.
[6] R.K. Hanson, G.A. Pang, S. Chakraborty, W. Ren, S. Wang, D.F. Davidson, Constrained reaction volume approach for studying chemical kinetics behind reflected shock waves, Combust. Flame 160 (9) (2013) 1550–1558.
[7] M. Campbell, A. Tulgestke, D. Davidson, R. Hanson, A second-generation constrained reaction volume shock tube, Rev. Sci. Instrum. 85 (5) (2014) 055108.
[8] V.A. Troutman, C.L. Strand, M.F. Campbell, A.M. Tulgestke, V.A. Miller, D.F. Davidson, R.K. Hanson, High-speed OH* chemiluminescence imaging of ignition through a shock tube end-wall, Appl. Phys. B 122 (3) (2016) 56.
[9] O. Pryor, S. Barak, B. Koroglu, E. Ninnemann, S.S. Vasu, Measurements and interpretation of shock tube ignition delay times in highly CO2 diluted mixtures using multiple diagnostics, Combust. Flame 180 (2017) 63–76.
[10] A. Tulgestke, S. Johnson, D. Davidson, R. Hanson, High-speed imaging of inhomogeneous ignition in a shock tube, Shock Waves 28 (5) (2018) 1089–1095.
[11] M. Figueroa-Labastida, J. Badra, A.M. Elbaz, A. Farooq, Shock tube studies of ethanol preignition, Combust. Flame 198 (2018) 176–185.
[12] A. Susa, D. Davidson, R. Hanson, Gravity-current-induced test gas stratification and its prevention in constrained reaction volume shock-tube experiments, Shock Waves 29 (7) (2019) 969–984.
[13] A.M. Ferris, A.J. Susa, D.F. Davidson, R.K. Hanson, High-temperature laminar flame speed measurements in a shock tube, Combust. Flame 205 (2019) 241–252.
[14] J. Shao, R. Choudhary, A.J. Susa, D.F. Davidson, R.K. Hanson, High-speed imaging of n-heptane ignition in a high-pressure shock tube, Proc. Combust. Inst. 38 (1) (2021) 911–918.
[15] D. Nativel, P. Niegemann, J. Herzler, M. Fikri, C. Schulz, Ethanol ignition in a high-pressure shock tube: ignition delay time and high-repetition-rate imaging measurements, Proc. Combust. Inst. 38 (1) (2021) 901–909.
[16] E. Ninnemann, O. Pryor, S. Barak, S. Neupane, Z. Loparo, A. Laich, S.S. Vasu, Reflected shock-initiated ignition probed via simultaneous lateral and endwall high-speed imaging with a transparent, cylindrical test-section, Combust. Flame 224 (2021) 43–53.

Please cite this article as: A.J. Susa and R.K. Hanson, Simultaneous side-wall-schlieren and -emission imaging of autoignition phenomena in conventional and constrained-reaction-volume shock-tube experiments, Proceedings of the Combustion Institute, https://doi.org/10.1016/j.proci.2022.08.063

[17] M. Figueroa-Labastida, A. Farooq, Simultaneous lateral and endwall high-speed visualization of ignition in a circular shock tube, Combust. Flame 214 (2020) 263–265.
[18] D. Nativel, P. Niegemann, J. Herzler, M. Fikri, C. Schulz, A study of ethanol oxidation in high-pressure shock tube: Ignition delay time measurements and high-speed imaging of the ignition process, 27th ICDERS, 2019. Beijing, China
[19] A.J. Susa, R.K. Hanson, Flame image velocimetry: seedless characterization of post-reflected-shock velocities in a shock tube, Exp. Fluids (2022).
[20] K. Grogan, M. Ihme, Stanshock: a gas-dynamic model for shock tube simulations with non-ideal effects and chemical kinetics, Shock Waves 30 (4) (2020) 425–438.
[21] Z. Hong, G.A. Pang, S.S. Vasu, D.F. Davidson, R.K. Hanson, The use of driver inserts to reduce non-ideal pressure variations behind reflected shock waves, Shock Waves 19 (2) (2009) 113–123.
[22] A.J. Susa, High-Speed Imaging Studies of Flames in a Shock Tube: Refined Techniques and New Applications, Stanford University, 2022 Ph.D. thesis.
[23] L. Zheng, A.J. Susa, R.K. Hanson, Methodology of designing compact schlieren systems using off-axis parabolic mirrors, Appl. Opt. 61 (2022) 4857–4864.
[24] G.S. Settles, Schlieren and shadowgraph techniques: visualizing phenomena in transparent media, Springer Science & Business Media, 2001, pp. 116–118.
[25] S. van der Walt, J.L. Schönberger, J. Nunez-Iglesias, F. Boulogne, J.D. Warner, N. Yager, E. Gouillart, T. Yu, the scikit-image contributors, Scikit-image: image processing in Python, PeerJ 2 (2014) e453.
[26] M.F. Campbell, K.G. Owen, D.F. Davidson, R.K. Hanson, Dependence of calculated postshock thermodynamic variables on vibrational equilibrium and input uncertainty, J. Thermophys. Heat Transf. 31 (3) (2017) 586–608.
[27] S. Wang, T. Parise, S.E. Johnson, D.F. Davidson, R.K. Hanson, A new diagnostic for hydrocarbon fuels using 3.41-um diode laser absorption, Combust. Flame 186 (2017) 129–139.
[28] Ottomatic GmbH, pycine, 2019, (https://github.com/ottomatic-io/pycine).
[29] J.D. Hunter, Matplotlib: a 2d graphics environment, Computing in Science & Engineering 9 (3) (2007) 90–95.
[30] K.P. Grogan, M. Ihme, Weak and strong ignition of hydrogen/oxygen mixtures in shock-tube systems, Proc. Combust. Inst. 35 (2) (2015) 2181–2189.
[31] J.T. Lipkowicz, I. Wlokas, A.M. Kempf, Analysis of mild ignition in a shock tube using a highly resolved 3d-LES and high-order shock-capturing schemes, Shock Waves 29 (4) (2018) 511–521.
[32] D.G. Goodwin, R.L. Speth, H.K. Moffat, B.W. Weber, Cantera: An object-oriented software toolkit for chemical kinetics, thermodynamics, and transport processes, 2021. Version 2.5.1.
[33] Q.-D. Wang, S. Panigrahy, S. Yang, S. Martinez, J. Liang, H.J. Curran, Development of multipurpose skeletal core combustion chemical kinetic mechanisms, Energy & Fuels (2021).
[34] U. of California at San Diego, Chemical-kinetic mechanisms for combustion applications, 2016.
[35] H. Wang, X. You, A.V. Joshi, S.G. Davis, A. Laskin, F. Egolfopoulos, C.K. Law, USC Mech Version II. High-temperature combustion reaction model of H2/CO/C1-C4 Compounds(2007).
[36] R.L. Belford, R.A. Strehlow, Shock tube technique in chemical kinetics, Annu. Rev. Phys. Chem. 20 (1) (1969) 247–272.
[37] G. Pang, D. Davidson, R. Hanson, Experimental study and modeling of shock tube ignition delay times for hydrogen–oxygen–argon mixtures at low temperatures, Proc. Combust. Inst. 32 (1) (2009) 181–188.
[38] J.T. Lipkowicz, D. Nativel, S. Cooper, I. Wlokas, M. Fikri, E. Petersen, C. Schulz, A.M. Kempf, Numerical investigation of remote ignition in shock tubes, Flow Turbul. Combust. 106 (2) (2020) 471–498.

Please cite this article as: A.J. Susa and R.K. Hanson, Simultaneous side-wall-schlieren and -emission imaging of autoignition phenomena in conventional and constrained-reaction-volume shock-tube experiments, Proceedings of the Combustion Institute, https://doi.org/10.1016/j.proci.2022.08.063